ACS APPLIED MATERIALS & INTERFACES

Research Article

www.acsami.org

Hybrid Colloidal Au-CdSe Pentapod Heterostructures Synthesis and Their Photocatalytic Properties

Krishna Kanta Haldar,[†] Godhuli Sinha,[‡] Jouko Lahtinen,[‡] and Amitava Patra*[,†]

[†]Department of Materials Science, Indian Association for the Cultivation of Science, Jadavpur, Kolkata 700032, India

[‡]Department of Applied Physics, Aalto University School of Science, FI-00076 Aalto, Finland

Supporting Information

ABSTRACT: In this report, we present a self-driven chemical process to design exclusive Au/CdSe pentapod heterostructures with Au core and CdSe arms. We have analyzed these heterostructures using high-resolution transmission electron microscope (HRTEM), high angle annular dark field-scanning transmission electron microscopic (HAADF-STEM), X-ray diffraction, and X-ray photoelectron spectroscopy (XPS) studies. Microscopic studies suggest that pentapod arms of CdSe are nucleated on the (111) facets of Au and linearly grown only along the [001] direction. From the XPS study, the shifting of peak positions in the higher binding energy region for Au/CdSe heterostructures compared to Au nanoparticles has been found which indicates the charge transfer from CdSe to Au in heterostructures. The steady state and time resolved spectroscopic studies unambiguously confirm the electron transfer from photoexcited CdSe to Au, and the rate of electron transfer is found to be 3.58×10^{8} s^{-1}. It is interesting to note that 87.2% of R6G dye is degraded by the Au/CdSe heterostructures after 150 min UV irradiation, and the apparent rate constant for Au/CdSe heterostructures is found to be 0.013 min^{-1}. This new class of metal-semiconductor heterostructures opens up new possibilities in photocatalytic, solar energy conversion, photovoltaic, and other new emerging applications.

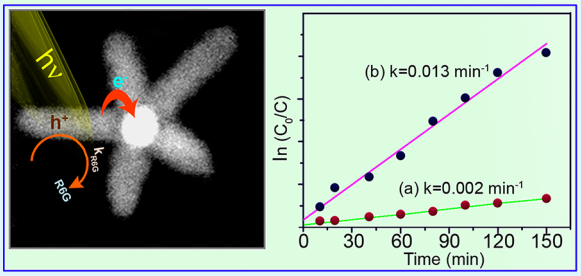

KEYWORDS: *metal semiconductor, hybrid, heterostructures, pentapods, photocatalytic, steady state*

INTRODUCTION

Extensive research efforts have been devoted to metal-semiconductor hybrid nanostructures to find out potential applications in the areas of photonic and optoelectronic because these nanostructures exhibit combined properties of metal and semiconductor.[1−5] These hybrid nanostructures can have various architectures, including individual metal conjugated with semiconductor spacer,[6] core-shell,[7] tetrapods,[8] and dumbbells shapes.[9] The design of metal semiconductor hybrid nanostructures leads to exciting opportunities for manipulating exciton dynamics for solar energy conversion and light harvesting applications. These unique classes of heterostructured materials are endowed with remarkable advantages as photocatalysts because of the low lying Fermi energy level of metal nanoparticles serve as a reservoir of photoelectrons and enhance the lifetime of photogenerated carriers, thus possibly enhancing the overall photocatalytic properties.

Different combined heterostructures of Au/CdSe,[7,10,11] Au/CdS,[12−14] Au-CdSe/CdS,[15] Au/PbS,[16] Au/-PbSe,[17] semiconductor rods with metal tips,[18] tetrapods with metal tips,[9] rods with decorative metal particles,[19] metal-semiconductor nanoflower,[20] metal core with semiconductor shell,[7] and vice versa[21] are already reported. Synthesis of these complex heterostructured materials is not straight forward like metal or semiconductor nanostructures; rather, it needs a more selective approach to bring both their counterparts together. For example, for the linear and branched heterostructures of Au/CdSe, CdSe rods, and tetrapods, the semiconductor parts are synthesized at higher temperature and metal tips are grown at room temperature.[9] However, the situation remains complicated for the reverse case to nucleate and grow the semiconductor counter parts of the heterostructures on metal surfaces which require a high temperature reaction system. To our knowledge, there is no report on pentapod metal-semiconductor heterostructures in the literature. Pentapod heterostructure with metal core and semiconductor arms which preferably needs the nucleation and growth of semiconductor arms on metal seeds at elevated temperature where the reactivity of metals with the anion present in the solution may also compete with the semiconductor formation. Hence, a more precisely controlled chemical reaction system is required to architect these heterostructured materials. Even though there are reports of such structures with metal Au core and semiconductor CdSe arm tetrapod structures in the literature,[10] their formation chemistry and the shape transformation processes are not yet clearly established. The core issue here is the fundamental understanding of the crystal growth at the junction between the atomic patterns AA of metals and AB of semiconductors. Once this would be achieved, the chemical reactions could be manipulated for the growth of semi-

Received: September 3, 2012
Accepted: October 31, 2012
Published: October 31, 2012

   dx.doi.org/10.1021/am301859b | ACS Appl. Mater. Interfaces 2012, 4, 6266−6272

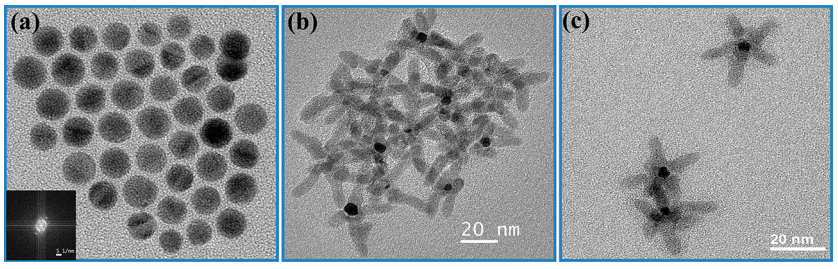

Figure 1. TEM images of seed Au (a) and Au/CdSe pentapod heterostructures (b and c).

conductor arms on metal seeds at elevated temperature to lead different complex heterostructures. The design of pentapod shaped heterostructures has been achieved by creating a buffer interface AuSe layer on the surface of gold seeds and immediately allowing the semiconductor CdSe to grow on them by introducing appropriate precursors within certain reaction time intervals.

In the present study, we report a facile and reproducible method for fabrication of Au-CdSe pentapod heterostructures with controllable reaction parameters and understand their photophysical properties, specially their photocalatytic properties. Such metal-semiconductor hybrid nanostructures should have great potentials for photocatalytic properties, nonlinear optical properties, photovoltaic devices, and chemical sensors.

EXPERIMENTAL SECTION

Materials. Chloroauric acid ($HAuCl_4 \cdot 3H_2O$, 99.9 %), cadmium oxide (CdO), selenium powder (Se), stearic acid (SA, 95%), trioctylphosphine (TOP, 90%), 1-octadecene (99%), tetraoctyl ammonium bromide (TOAB, Fluka), and 1-dodecylamine (DDA, 98%) were purchased from Aldrich, and sodium borohydride ($NaBH_4$), toluene (chemical grade), *n*-hexane (analytical grade), methanol (analytical grade), and ethanol (analytical grade) were purchased from Merck India Ltd. All of the reagents were used without further purification.

Preparation of Stock Solutions. *Cadmium Stearate Solution.* CdO (0.15 mmol) and stearic acid (SA, 350 mg) were mixed in 10 mL of 1-octadecene, and this mixture was heated to 250 °C under vigorous stirring and kept at 180 °C for 20 min under Ar flow. After the solution became clear, the temperature was reduced to room temperature, and this solution was kept for Cd precursor.

TOP-Se Solution. A solution of TOP-Se was prepared by dissolving selenium (0.3 mmol) in a mixture of trioctylphosphine (TOP) (3 mL) and 1-octadecene (3 mL) at 50 °C under stirring condition.

Synthesis of Gold Nanoparticles. Gold nanoparticles were synthesized via modification of a literature protocol.[22] Briefly, an aqueous solution of $HAuCl_4 \cdot 3H_2O$ (1 mM, 10 mL) was added to a solution of TOAB in toluene (5 mM, 10 mL). The yellow aqueous phase became colorless, and the toluene phase turned orange as a result of phase transfer and complexion of $[AuCl_4]^-$ with tetraoctylammonium cations. After the Au precursor was transferred to the toluene layer, the organic phase was separated and mixed with 0.202 g of dodecylamine in 5 mL of toluene. After stirring for 10 min at room temperature, a freshly prepared aqueous solution of sodium borohydride, $NaBH_4$ (10 M, 1 mL), was added drop-wise into the reaction mixture for a period of 2 min, after which the mixture was vigorously stirred for an additional 10 min. Subsequently, Au nanoparticles were precipitated from toluene by adding ethanol and acetone followed by centrifugation. The nanoparticles were re-dispersed in 10 mL of toluene. For this particular procedure, the Au nanoparticles were about 5 nm in diameter, with nearly spherical shape.

Synthesis of Noble Gold/Cadmium Selenide Pentapod Heterostructures. In a typical synthesis, 5 mL of stock gold solution has been dissolved with 5 mL of toluene and added to the reaction mixture having 0.014 g of dodecyl amine and 10 mL of ODE. The solution is heated to ~100°C and purged with Argon to remove all the toluene from the reaction flask. After 20 minutes, the reaction temperature has been raised to 280 °C and 0.5 mL of stock TOP-Se solution has been injected. After 50 s, 1 mL of cadmium stock solution has been injected. After annealing at this temperature for 5 min, the final product Au/CdSe was purified by adding small amounts of methanol/acetone mixture followed by centrifugation at 4000 rpm and redispersed again in chloroform for further experiment.

Photocatalytic Studies. For photocatalytic measurement, the surface of as-synthesized Au/CdSe pentapods must be exchanged with MPA to transferred aqueous solution. For this, 0.5 mL of MPA is dissolved in 15 mL of double distilled water, and subsequently, the pH of the solution was increased to 10 by adding 5 M sodium hydroxide; then, 30 mL of Au/CdSe nanopentapod nanocrystals (in chloroform) were added to this solution under stirring, resulting in a two-phase system (water above chloroform). After phase transferring, 4 mL of diethyl ether and 4 mL of ethyl acetate were added to this mixture, and then, 10 mL of methanol was added. After centrifugation, the precipitate was washed by methanol and re-dissolving in 10 mL of double distilled water. The photocatalytic activity of the as-prepared samples was tested by de-colorization of Rhodamine6G (R6G) dye molecule in aqueous solution at room temperature under UV light. The experiments were as follows: 20 mL of Au/CdSe pentapod heterostructures aqueous solution was added to 50 mL of 2.18×10^{-6} mM aqueous solution of R6G dye; the mixture was stirred in the dark for 30 min to attain the adsorption−desorption equilibrium. In given time intervals, analytical solution samples were taken from the suspension and immediately centrifuged at 12 000 rpm for 6 min. The quantity of dye in the solution was determined by measuring the absorption intensity at 525 nm, which is the main absorption peak of R6G dye.

Instrumentation. *Optical Study.* Absorption and fluorescence spectra of Au/CdSe pentapod nanocrystals were taken at room temperature with a Shimadzu UV-2450 UV-VIS spectrometer and a Horiba Jobin Yvon Fluoro Max-P fluorescence spectrometer, respectively [resolution of the instrument = 0.3 nm; accuracy = ± 0.5 nm]. For the time correlated single photon counting (TCSPC) measurements, the samples were excited at 370 nm using a picoseconds LED (IBH Nanoled-07) in an IBH Fluorocube apparatus. The typical full width at half-maximum (fwhm) of the system response using a liquid scatter is about 300 ps. The repetition rate is 1 MHz. The fluorescence decays were collected on a Hamamatsu MCP photomultiplier (C487802). The fluorescence decays were analyzed using IBH DAS6 software. The following expression was used to analyze the experimental time-resolved fluorescence decays, $I(t)$:

$$I(t) = \sum_{i}^{n} \alpha_i \exp(-t/\tau_i) \quad (1)$$

Here, n is the number of discrete decay components and α_i and τ_i are the pre-exponential factors and excited-state fluorescence lifetimes associated with the i^{th} component, respectively. The average decay time

$$\langle \tau \rangle = \sum_{i=1}^{n} b_i \tau_i \quad (2)$$

where $b_i = ((\alpha_i)/(\sum_i \alpha_i))$, standard deviation error = ± 10%.

XRD. The crystalline phase of the nanoparticles was studied by X-ray diffraction patterns (Rich-Seifert XRD 3000P). X-ray photoelectron spectroscopy (XPS) was recorded with a SSX-100 ESCA spectrometer using Al Kα (1486.6 eV) line and spot size of 600 μm.

TEM and High-Resolution Transmission Electron Microscope. JEOL-TEM-2010 has been used for high-resolution transmission electron microscope (HRTEM) images (operating voltage at 200 kV).

High Angle Annular Dark Field-Scanning Transmission Electron Microscopic Images. High angle annular dark field-scanning transmission electron microscopic (HAADF-STEM) images were taken by an ultra high resolution field emission gun transmission electron microscope (JEOL 300 kV).

RESULTS AND DISCUSSION

Figure 1a shows a typical bright field TEM image of the as-synthesized monodispersed seed spherical gold nanoparticles with an average diameter of about 5 ± 0.6 nm. The inset of Figure 1a is the corresponding FFT pattern of pure gold. The TEM images of Au/CdSe pentapod heterostructures are shown Figures 1b,c where Au nanoparticles are in the center and the arms are CdSe. Some of these multipods are very similar to previously reported[23] Au/CdS and Au/CdSe multipod heterostructures. Figure 2a shows a high-resolution TEM image of a single Au nanoparticle, where the lattice fringes are separated by distance, d = 2.35 Å, corresponding to the (111) plane of fcc cubic of Au NP. Figure 2b shows a hybrid Au/CdSe pentapod structure where the dark contrasts Au core has been clearly visible and all the five arms are shown in one plane with distinct separation. Figure 2c shows a closer view of the pentapod structure and the *d*-spacing that all of these arms are in wurtzite CdSe structures which are grown along [001] direction. Due to the difference in contrast of Au and CdSe and the orientation of the different arms relative to the electron beam, it is always difficult to observe clearly both lattice images of Au and CdSe simultaneously. However, we could verify the presence of the Au lattice in the center (Figure 2d) and the CdSe lattice in the arms (Figure 2c) under different imaging conditions. Banin et al.[9] have already reported that it is difficult to identify the interface between Au and CdSe, and they proposed the formation of Au−Se bonds[24] in the interface upon injection of Se before Cd precursor. Again, Felice et al.[25] showed that formation of AuSe due to mixing between Au and Se orbitals. Thus, we believe that a similar situation should be expected in the present study. The formation of this AuSe layer might help to form the pentapod heterostructures formation. For further information, we have analyzed these heterostructures using FFT, HAADF-STEM, XRD, and XPS studies. Figure 3 shows the HRTEM, selected area FFT, inverse FFT, and the *d*-spacing of the center of Au in pentapod structure, which again confirm the presence of gold at the center. It has been observed that this growth occurs on (111) facets of the cubic (fcc) gold and the junction is formed between the [001] axis of the wurtzite CdSe and [111] of fcc gold. HAADF-STEM images of the pentapod structures clearly suggest the formation of pentapod heterostructures with Au core and CdSe arms (Figure 4). Sometimes, we did not observe Au core because of the 3D structure of Au/CdSe pentapods, where CdSe arms are orientated in different planes. It is clearly observed from the arm patterns that pentapod arms of CdSe are nucleated on the (111) facets of Au and are linearly grown only along the [001] direction. To know the composition of Au/CdSe pentapod hybrid structures, we have carried out XRD and XPS measurement. The XRD pattern of the Au−CdSe pentapod heterostructures (Supporting Information S1) confirms that both cubic Au and wurtzite CdSe diffractions are present. Furthermore, the chemical composition of the Au/CdSe pentapod heterostructures is confirmed by the XPS spectra of the Cd-3d, Se-3d, and Au-4f electrons. A wide range of XPS measurements of Au/CdSe pentapod, CdSe nanoparticles, and Au nanoparticles is shown in Figure 5a. Notably, all the samples display strong O 1s and C1s peaks at ~531.5 and ~284 eV, presumably due to the organic ligands/solvent attached to the surface; however, no other impurities are detected. The Au photoemission spectra are deconvoluted into a doublet centered at 83.4 and 87.2 eV (Figure 5b) attributed to the

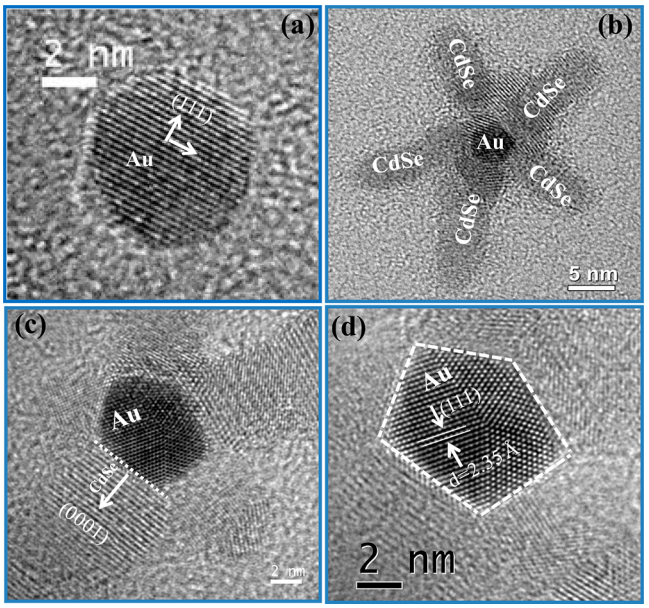

Figure 2. TEM and HRTEM images of Au and Au-CdSe pentapod shaped heterostructures: (a) a spherical Au seed, (b) a single pentapod shaped heterostructure image, (c) the HRTEM image of a pentapod and the lattice planes matches with wurtzite CdSe, and (d) a close view of a pentapod center (Au) where the growth of CdSe from [111] direction of Au NP.

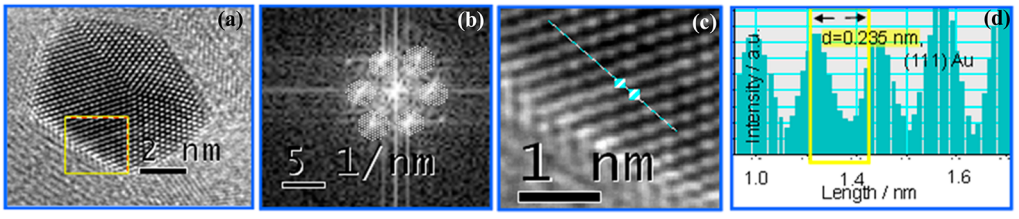

Figure 3. HRTEM (a), selected area FFT (b), inverse FFT (c), and height profile of the center Au (d) of the pentapod heterostructures.

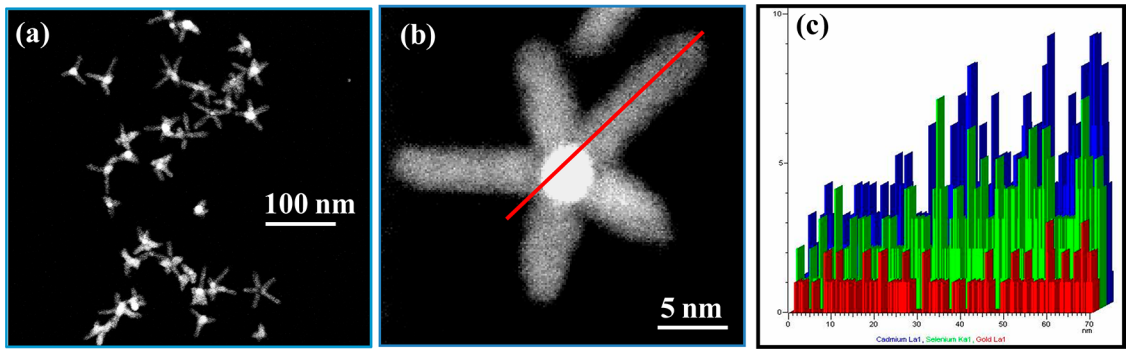

Figure 4. (a) HAADF image with the larger area magnification, (b) smaller area HAADF-STEM image, and (c) the line scan electron mapping for the presence of Au.

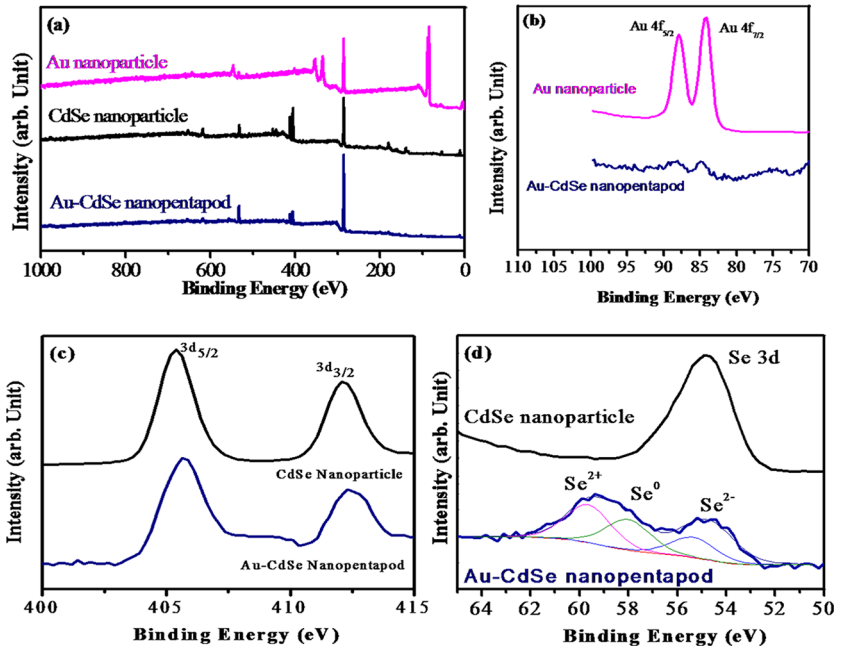

Figure 5. (a) Photoemission spectra of Au-CdSe nanopentapod, CdSe nanoparticles, and Au nanoparticles, (b) photoemission of $4f_{7/2}$ and $4f_{5/2}$ orbital of Au in Au NP and Au/CdSe pentapod heterostructures, (c) Cd 3d peaks of $3d_{5/2}$ and $3d_{3/2}$, and (d) Se 3d in CdSe QD and Au/CdSe pentapod heterostructures.

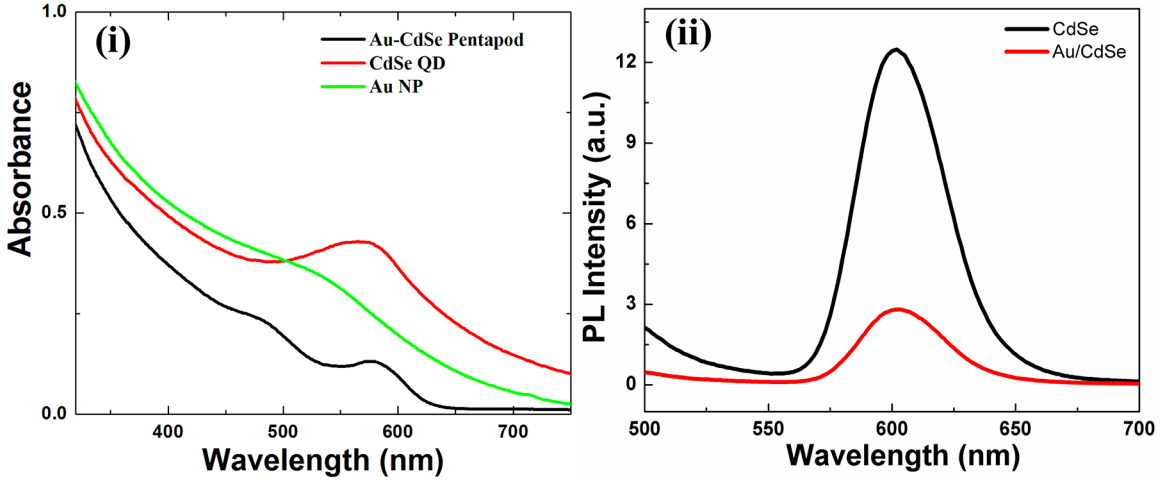

Figure 6. (i) Optical absorption spectra and (ii) PL spectra of CdSe and Au/CdSe pentapod heterostructures.

Au $4f_{7/2}$ and Au $4f_{5/2}$, respectively, with a fixed FWHM (≈1.8 eV) value. The size of the nanostructures is probably responsible for the broadening of these peaks. The absence of a band attributed to Au^+ at 84.9 eV indicates that the Au

dx.doi.org/10.1021/am301859b | ACS Appl. Mater. Interfaces 2012, 4, 6266−6272

atoms are in metallic form in this core-shell nanostructure.[26,27] Au 4f signals for the Au/CdSe pentapod is quenched compared to Au nanoparticles, which indicates that, in former case, Au nanoparticles are underneath the CdSe layer. A shift of peak position in a higher binding energy region for Au/CdSe heterostructures compared to Au nanoparticle indicates the charge transfer from CdSe to Au. Cd 3d peaks can be deconvoluted into a doublet representing $3d_{5/2}$ and $3d_{3/2}$ at 405.0 and 412 eV, respectively (FWHM ≈ 1.70 eV, Figure 5c), which suggests that Cd is in 2+ oxidation state. Atomic ratios of Au, Cd, and Se in all the samples are incorporated in Table S1, Supporting Information. In the case of both CdSe QDs and pentapod, Cd/Se intensity ratio differs from 1:1 because Se 3d is less sensitive than Cd 3d. Se 3d (Figure 5d) region shows two well-resolved peaks representing three different states attributed to Se^{2-} (reduced), Se^0 (neutral), and Se^{2+} (oxidized) states at 54, 58, and 61 eV. The presence of Se^0 and Se^{2+} oxidation states in the case of Au/CdSe pentapod indicates the charge transfer from CdSe to Au.[28]

The absorption and photoluminescence spectra of CdSe and Au/CdSe pentapod heterostructures are shown in Figure 6i,ii, respectively. The absorption spectra of both CdSe and Au change significantly upon forming directly coupled Au/CdSe heterostructures. It is to be noted that there is a spectral overlap between the surface plasmon bands of Au nanoparticles (501 nm) with the emission band of CdSe QD (peak at 598 nm). Thus, the observed significant quenching of CdSe PL emission in Au/CdSe hybrid nanostructure is due to electron transfer from CdSe to Au because it is well established that Au nanoparticles promote the interfacial charge transfer processes.[29]

To further confirm the electron-transfer process in Au/CdSe heterostructure, the decay times of pure CdSe QD and the Au/CdSe pentapod heterostructures have been measured using time correlated single photon counting (TCSPC). Figure 7

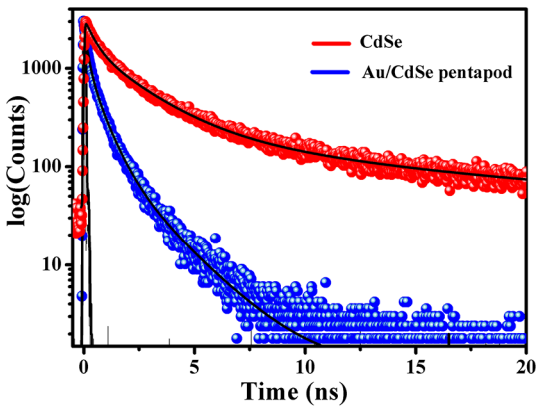

Figure 7. Decay profiles of CdSe and Au/CdSe pentapod heterostructures.

shows the decay curves of CdSe and Au/CdSe heterostructures under 370 nm excitation. The decay profile of CdSe is fitted most reasonably by a tri-exponential model(Table S2, Supporting Information). The fitting shows that the fast component, τ_1 (1.16 ns), that possibly arises from the free exciton states,[30] which is the major deactivation pathway (58.5%), shortens to 0.55 ns in the Au/CdSe NPs. The exciton lifetime of CdSe is 6.96 ns and, in the Au/CdSe nanocomposites, is found to be 1.97 ns. The shortening of decay time suggests that electron transfer from CdSe to Au in Au/CdSe pentapod heterostructures correlated with the PL quenching data. The electron-transfer rate constant (k_{ET}) in Au/CdSe heterostructure is estimated using the following equation:

$$k_{ET} = 1/\tau_{Au/CdSe} - 1/\tau_{CdSe} \quad (3)$$

and it is found to be 3.58×10^8 s^{-1}. The steady state and time resolved spectroscopic studies unambiguously confirm that electrons transfer from photoexcited CdSe to Au.

It is well known[31] that the Fermi level of Au is more positive (E_F = 0.5 V vs. NHE) compared to the conduction band energy of CdSe (E_{CB} = −1.2 V vs NHE). Thus, the charge transfer from the excited CdSe to Au nanoparticles would be thermodynamically favorable. Hence, the injection of electrons from CdSe to Au leads to storage of electrons in the Au core using following equations;

$$CdSe + hv \rightarrow CdSe(e + h) \quad (4)$$

$$Au/CdSe + e \rightarrow Au(e)/CdSe(h) \quad (5)$$

Finally, we have examined the oxidative photocatalytic activity of the Au/CdSe pentapod heterostructures with Rhodamine 6G (R6G), which is known to undergo oxidative degradation in water. Figure 8 shows the results of photodegradation of Rhodamine 6G dye (R6G) under UV irradiation (365 nm) in the presence of CdSe and as-prepared Au/CdSe pentapod samples. Rhodamine 6G dye shows a major absorption band at 525 nm in aqueous solution. It is found that the absorbance is gradually reduced with increased UV irradiation time for the Au/CdSe heterostructure. It clearly shows the process is slower in the case of pure CdSe nanocrystal. Figure 8i shows the R6G dye decomposition rate as a function of UV irradiation time. Pure CdSe nanocrystal and Au/CdSe heterostructures are tested for 150 min under identical conditions. It is found that 87.2% of R6G dye is degraded by the Au/CdSe heterostructures after 150 min UV irradiation, whereas 27.3% degradation is observed in the case of pure CdSe nanocrystals. The decomposition of R6G dye under the same UV irradiation condition is negligible in the absence of both CdSe nanocrystals and Au/CdSe heterostructures. Degradation rate k_D is calculated using following equation:

$$k_D = (A_0 - A)/A_0 \quad (6)$$

where A_0 and A were the initial absorbance and the sample absorbance, respectively. The kinetic profiles of degradation of R6G under UV light are also investigated. The photodegradation of R6G follows apparently first-order kinetics. Its kinetics can be expressed as $\ln(C_0/C) = kt$, where k is the apparent reaction rate constant, C_0 is the concentration of R6G at adsorption equilibrium, and C is the residual concentration of R6G at different illumination intervals. Figure 8ii shows a linear relationship between $\ln(C_0/C)$ and reaction time (t), indicating that the investigated photodegradation of R6G follows a first-order kinetics model. The apparent rate constants as kinetic evidence for the samples are determined as 0.002 and 0.013 min^{-1} for CdSe and Au/CdSe, respectively. Thus, the photocatalytic activity enhances due to Au/CdSe heterostructures. These results clearly demonstrate that the Au/CdSe heterostructures have significantly improved photocatalytic activities in comparison with CdSe nanocrystals. Thus, the Au/CdSe heterostructures improve the separation of photogenerated electron-hole pairs due to the potential

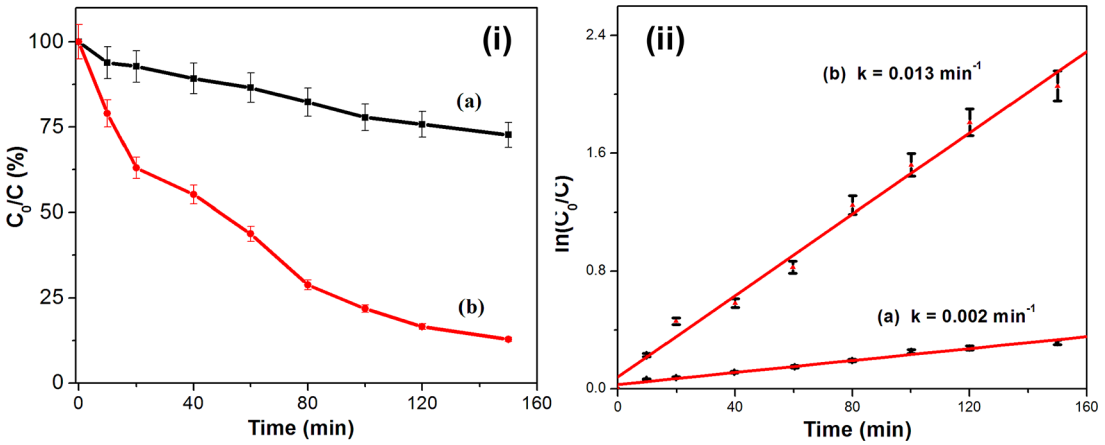

Figure 8. (i) Photodegradation and (ii) rate of photodegradation of R6G dye in presence of (a) CdSe and (b) Au/CdSe heterostructures under UV light.

energy differences between Au and CdSe, thus enhancing the photocatalytic activity.

CONCLUSION

In summary, a novel chemical approach for the synthesis of pentapod heterostructures with metal Au seed and semiconductor CdSe arms and its formation chemistry have been discussed. The growth mechanism of the semiconductor CdSe on the surface of noble metal gold seeds during the formation of the Au-CdSe pentapod heteronanostructures is investigated. Au core in these pentapod structures caused the material to exhibit significant improvement in the photocatalytic activity. The design of new optical-based materials based on metal-semiconductor heterostructures has opened up new possibilities for photocatalytic and optoelectronic applications. Although many issues are to be addressed, the general interest in metal-semiconductor heterostructures is expected to grow in coming years because applications are still in the embryonic stage.

ASSOCIATED CONTENT

Supporting Information

XRD patterns of CdSe QD and Au/CdSe pentapod heterostructure; atomic ratios of Au, Cd, and Se in the samples; Au nanoparticles, CdSe QDs, and Au-CdSe pentapod from XPS measurements; time resolved fluorescence studies and photodegration of R6G dye solution in the presence Au/CdSe pentapod heterostructure. This information is available free of charge via the Internet at http://pubs.acs.org.

AUTHOR INFORMATION

Corresponding Author

*E-mail: msap@iacs.res.in. Phone: (91)-33-2473-4971. Fax: (91)-33-2473-2805.

Notes

The authors declare no competing financial interest.

ACKNOWLEDGMENTS

A.P. would like to acknowledge support from "DAE-SRC Outstanding Investigator Awards".

REFERENCES

(1) Li, Y.-Q.; Guan, L.-Y.; Zhang, H.-L.; Chen, J.; Lin, S.; Ma, Z.-Y.; Zhao, Y.-D. *Anal. Chem.* **2011**, *83*, 4103.
(2) Jen-La Plante, I.; Habas, S. E.; Yuhas, B. D.; Gargas, D. J.; Mokari, T. *Chem. Mater.* **2009**, *21*, 3662.
(3) Costi, R.; Saunders, A. E.; Elmalem, E.; Salant, A.; Banin, U. *Nano Lett.* **2008**, *8*, 637.
(4) Shaviv, E.; Banin, U. *ACS Nano* **2010**, *4*, 1529.
(5) Sametband, M.; Shweky, I.; Banin, U.; Mandler, D.; Almog, J. *Chem. Commun.* **2007**, *11*, 1142.
(6) Pons, T.; Medintz, I. L.; Sapsford, K. E.; Higashiya, S.; Grimes, A. F.; English, D. S.; Mattoussi, H. *Nano Lett.* **2007**, *7*, 3157.
(7) Zhang, J.; Tang, Y.; Lee, K.; Ouyang, M. *Science* **2010**, *327*, 1634.
(8) Yong, K.-T.; Sahoo, Y.; Swihart, M. T.; Prasad, P. N. *Adv. Mater.* **2006**, *18*, 1978.
(9) Mokari, T.; Rothenberg, E.; Popov, I.; Costi, R.; Banin, U. *Science* **2004**, *304*, 1787.
(10) Figuerola, A.; van Huis, M.; Zanella, M.; Genovese, A.; Marras, S.; Falqui, A.; Zandbergen Henny, W.; Cingolani, R.; Manna, L. *Nano Lett.* **2010**, *10*, 3028.
(11) Tian, Z.-Q.; Zhang, Z.-L.; Jiang, P.; Zhang, M.-X.; Xie, H.-Y.; Pang, D.-W. *Chem. Mater.* **2009**, *21*, 3039.
(12) Khon, E.; Hewa-Kasakarage, N. N.; Nemitz, I.; Acharya, K.; Zamkov, M. *Chem. Mater.* **2010**, *22*, 5929.
(13) Li, M.; Yu, X.-F.; Liang, S.; Peng, X.-N.; Yang, Z.-J.; Wang, Y.-L.; Wang, Q.-Q.. *Adv. Funct. Mater.* **2011**, *21*, 1788.
(14) Khon, E.; Mereshchenko, A.; Tarnovsky Alexander, N.; Acharya, K.; Klinkova, A.; Hewa-Kasakarage Nishshanka, N.; Nemitz, I.; Zamkov, M. *Nano Lett.* **2011**, *11*, 1792.
(15) Shi, W.; Zeng, H.; Sahoo, Y.; Ohulchanskyy, T. Y.; Ding, Y.; Wang, Z. L.; Swihart, M.; Prasad, P. N. *Nano Lett.* **2006**, *6*, 875.
(16) Talapin, D. V.; Yu, H.; Shevchenko, E. V.; Lobo, A.; Murray, C. B. *J. Phys. Chem. C* **2007**, *111*, 14049.
(17) Carbone, L.; Kudera, S.; Giannini, C.; Ciccarella, G.; Cingolani, R.; Cozzoli, P. D.; Manna, L. *J. Mater. Chem.* **2006**, *16*, 3952.
(18) Menagen, G.; MacDonald, J. E.; Shemesh, Y.; Popov, I.; Banin, U. *J. Am. Chem. Soc.* **2009**, *131*, 17406.
(19) Lee, J.; Govorov, A. O.; Dulka, J.; Kotov, N. A. *Nano Lett.* **2004**, *4*, 2323.
(20) AbouZeid, K. M.; Mohamed, M. B.; El-Shall, M. S. *Small* **2011**, *7*, 3299.
(21) Yang, J.; Ying, J. Y. *Nat. Mater.* **2009**, *8*, 683.
(22) Prasad, B. L. V.; Stoeva, S. I.; Sorensen, C. M.; Klabunde, K. J. *Chem. Mater.* **2003**, *15*, 935.
(23) Figuerola, A.; Franchini, I. R.; Fiore, A.; Mastria, R.; Falqui, A.; Bertoni, G.; Bals, S.; Tendeloo, G.V.; Kudera, S.; Cingolani, R.; Manna, L. *Adv. Mater.* **2009**, *21*, 550.
(24) Cretier, J. E.; Wiegers, G. A. *Mater. Res. Bull.* **1973**, *8*, 1427.
(25) de Paiva, R.; Di Felice, R. *ACS Nano* **2008**, *2*, 2225.
(26) Brust, M.; Walker, M.; Bethell, D.; Schiffrin, D. J.; Whyman, R. *J. Chem. Soc. Chem. Comm.* **1994**, 801.
(27) Ertas, G.; Demirok, U. K.; Suzer, S. *App. Surf. Sci.* **2005**, *249*, 12.

(28) Bhandari, S.; Deepa, M.; Sharma, S. N.; Joshi, A. G.; Srivastava, A. K.; Kant, R. *J. Phys. Chem. C* **2010**, *114*, 14606.
(29) Kim, J.; Lee, D. *J. Am. Chem. Soc.* **2007**, *129*, 7706.
(30) Hosoki, K.; Tayagaki, T.; Yamamoto, S.; Matsuda, K.; Kanemitsu, Y. *Phys. Rev. Lett.* **2008**, *100*, 207404/1−207404/4.
(31) Jakob, M.; Levanon, H.; Kamat, P. V. *Nano Lett.* **2003**, *3*, 353.